Journal of Food Engineering 375 (2024) 112060

Contents lists available at ScienceDirect

Journal of Food Engineering

journal homepage: www.elsevier.com/locate/jfoodeng

Effect of atmospheric pressure changes on gas transmission through microperforated packages of respiring products

Sara Vega-Diez [a,b], María Luisa Salvador [b,*], Jaime González-Buesa [a,b]

[a] Departamento de Ciencia Vegetal, Centro de Investigación y Tecnología Agroalimentaria de Aragón (CITA), Instituto Agroalimentario de Aragón - IA2 (CITA-Universidad de Zaragoza), Av. Montañana 930, 50059, Zaragoza, Spain
[b] Grupo de Investigación en Alimentos de Origen Vegetal, Universidad de Zaragoza, Instituto Agroalimentario de Aragón-IA2-(Universidad de Zaragoza-CITA), Miguel Servet 177, 50013, Zaragoza, Spain

ARTICLE INFO

Keywords:
Barometric pressure
Mathematical model
Microperforation
Modified atmosphere packaging
Transportation
Weather

ABSTRACT

The objective of this work was to quantify the effect of atmospheric pressure changes on gas transmission through microperforations, in order to understand the role of fluctuations in the atmospheric pressure on the headspace composition of microperforated modified atmosphere packages. A 3D numerical model that considers the spatial-time and pressure dependence of the gas composition was adapted to simulate the gas exchange through microperforations at different fixed pressures and at variable pressure due to atmospheric pressure fluctuations (such as those caused by atmospheric tides or by the development of high and low-pressure systems) or to changes in altitude during land or air transport. The model results were successfully verified with experimental data recorded in an experimental system built to measure the CO_2 exchange through microperforations affected by pressure changes due to weather conditions (the root mean squared error of the CO_2 composition was 0.01%). The results reveal the importance of contemplating the convective flow generated by a change in pressure outside the package. In the simulated routes, the difference in CO_2 concentration between considering the pressure-driven flow and neglecting it is one order of magnitude in a 10-h land transport through a medium mountain route, for a 1250 mL container with a single microperforation of 7420.6 μm^2 area and initial CO_2 concentrations on both sides of the hole of 0.05% and 20.95%. The air transport simulations showed that it is not enough to consider the difference in altitude between the cities of origin and destination, but rather all the pressure fluctuations along the route must be included in the model.

1. Introduction

Modified atmosphere packaging (MAP) technology plays an important role in extending the shelf-life of fresh and fresh-cut produce, since MAP systems are capable of maintaining the product quality if the temperature and gas composition (in general, low levels of O_2 and moderate levels of CO_2) are properly selected (Belay et al., 2016). Thus, MAP technology faces the challenge of adapting the gas composition inside the container to the requirements of each product, considering gas exchange through the package and the respiration rate of the packaged product. However, the optimum packaging atmosphere is not always achieved, fundamentally because the permeability to CO_2 of plastic packaging materials is 3–6 times greater than that of O_2 (Singh and Singh, 2005), while the ratio between CO_2 production and O_2 consumption in fresh produce is usually between 0.7 and 1.3 (Kader et al., 1989). This results in anaerobic conditions to achieve the CO_2 concentration necessary for antimicrobial benefits. An alternative to solve these drawbacks is the use of packages with perforations or tubes inserted. In these packages, the gas exchange with the outside takes place mainly through the perforations or tubes, and as the molecular diffusivities of the gases involved in air are similar, the CO_2/O_2 transfer ratio is reduced (González et al., 2008; Larsen and Liland, 2013).

Many factors are involved in the development of the gas composition inside microperforated packages: temperature and relative humidity (Del-Valle et al., 2003; Pandey and Goswami, 2012; Sonawane et al., 2022), perforation number and diameter (Castellanos et al., 2016; Chung et al., 2003; Del-Valle et al., 2003; González-Buesa et al., 2009; Larsen and Liland, 2013; Pandey and Goswami, 2012; Renault et al., 1994; Sonawane et al., 2022; Sousa-Gallagher and Mahajan, 2013; Winotapun et al., 2023; Xanthopoulos et al., 2012), air velocity outside

* Corresponding author.
E-mail address: mlsalva@unizar.es (M.L. Salvador).

https://doi.org/10.1016/j.jfoodeng.2024.112060
Received 14 December 2023; Received in revised form 18 March 2024; Accepted 20 March 2024
Available online 25 March 2024

the package (Sonawane et al., 2022), convective flow through the perforation (González-Buesa and Salvador, 2022), and configuration and location of the perforations (Giannoulis et al., 2017; Ramos et al., 2019). However, to the best of our knowledge, the influence of the atmospheric pressure or the presence of pressure variations in the gas exchange of microperforated MAP has not been analyzed.

Pressure changes in MAP systems may be generated by the differences between oxygen consumption and carbon dioxide production due to respiratory metabolism, the unevenly balanced permeation rates of the gases through the package, the condensation of moisture on the internal surface of the package, the absorption of gases by the water contained in the product, or the presence of gas scavengers, among other internal factors. These pressure variations may also be motivated by external factors including weather changes, atmospheric tides, and temperature and altitude variations during distribution of the packages. In MAP systems, the transport during distribution of the products may be subject to several of these factors, and therefore the pressure inside and outside the package evolves continuously. Thus, considering pressure or pressure variations may play an important role in the development of perforation-mediated MAP models with improved performance.

Additionally, in packages with perforations or tubes, these pressure differences on both sides of the package are compensated by a convective flow through the perforation causing a gas concentration profile around the hole, different from those existing in the rest of the container. The magnitude of the velocity field in the airstream going through the perforation may be especially high in the case of microperforated packages (perforation diameter between 50 and 300 μm). This convective flow through the perforation has been included in some of the mathematical models developed (Del-Valle et al., 2003; González-Buesa et al., 2009; Paul and Clarke, 2002; Ratti et al., 1998; Rennie and Tavoularis, 2009a). In other models based on Fick's law, a correction term, dependent on the hole diameter, has been included in the path length to account for concentration gradients around the perforation (Chung et al., 2003; Fishman et al., 1996; Ghosh and Anantheswaran, 2001; Giannoulis et al., 2017; Lange et al., 2000; Lee and Renault, 1998; Mistriotis et al., 2016; Paul and Clarke, 2002). However, very few models considering the spatial dependence of the gas concentrations in the headspace have been developed. Exceptions are the models developed by González-Buesa and Salvador (2022), Rennie and Tavoularis (2009b), applied to tubes, and by Giannoulis et al. (2017), but the latter case does not include the convective flow term.

Thus, the main objectives of this work were: i) to verify experimentally that changes in atmospheric pressure affect the gas transport through a microperforated package, and ii) to predict by means of a mathematical model how the gas exchange through the microperforated package is affected by pressure and/or pressure changes due to altitude variations during package transportation. To achieve these goals, an experimental system was designed to quantify in isolation the effect of atmospheric pressure on gas exchange through microperforations. In addition, a previously developed 3D mathematical model (González-Buesa and Salvador, 2022) was applied to predict the gas exchange through perforations due to both diffusive and convective flow, considering the spatial-time and pressure dependence of the gas composition.

2. Material and methods

2.1. Experimental system

An experimental set-up was of designed to analyze specifically the effect atmospheric pressure fluctuations on the gas exchange through a microperforation. The experimental system allows quantifying the evolution of the gas composition in a rigid package, with a single microperforation, in the absence of product, and with a wide concentration gradient between the package's headspace and outside, thus the measurements would not be affected by the metabolic activity of the product or by changes in the volume of the package. Extrapolating the results to a real MAP of fruits or vegetables would involve considering other factors such as changes in volume in the case of flexible packaging, the product's respiration rate and respiratory quotient, its tolerance to CO_2, and thus the desired concentration of CO_2 inside the package, the absorption of CO_2 within the product, as well as the number, distribution, and size of the microperforations, among others. Depending on these factors, the influence of atmospheric pressure changes on the gas composition of the headspace of the package may be more or less pronounced. However, the conclusions derived from the results obtained in the experimental system can be taken into account to more accurate estimation of gas exchange through microperforated packages. The system, shown in Fig. 1, is essentially made up of two units: a module in which gas exchange takes place through the microperforation under dynamic conditions and a module for pressure monitoring. The gas exchange module consists of: a cylindrical and acrylic upper chamber through which a mixture of 21% CO_2 – 79% N_2 flows at 100 mL min^{-1} by means of a diffuser, using a mass flow controller (Brooks Instrument model 5850 TR, Hatfield, PA, USA); and a lower 1250 mL glass chamber that initially contains atmospheric air (Familia Wiss Terrines, Le Parfait, Auvergne, France). The lid that separates both chambers has an 8 mm diameter hole where the film containing the perforation is glued. The CO_2 concentration that passes through the microperforation is measured with two sensors, one for CO_2 concentrations lower than 10,000 ppm (k30) and the other for higher concentrations (k33 ICB 30%), both from Senseair AB (Delsbo, Sweden). To achieve the tightness of the system, a press system gripping the two chambers was custom-built. The module for pressure monitoring is a glass jar similar to the lower chamber of the interchange gas module, but it is provided with a sensor to measure the differential pressure between the pressure inside the module and the atmospheric pressure (AMS 5915-100-D-B, Analog Microelectronics GmbH, Mainz, Germany), and thus accurately records small fluctuations in atmospheric pressure. The system also has an absolute pressure sensor to monitor atmospheric pressure (AMS 5915-1200-B, Analog Microelectronics GmbH, Mainz, Germany). The data gathered from the four sensors were transmitted every minute through an Arduino UNO (Arduino SRL, Strambino, Italy) to a laptop using the freeware software CoolTermWin (Roger Meier, CA, USA). The CO_2, atmospheric pressure and differential pressure evolution was determined for two different elliptical microperforations (major axis of 124.3 ± 0.8 μm and minor axis of 75.5 ± 0.6 μm, and measured area of 7420.6 ± 53.7 μm^2) during 300 h in sixtuplicate in order to obtain data for different weather conditions.

2.2. Mathematical model

The mathematical model developed by González-Buesa and Salvador (2022), implemented in the software COMSOL Multiphysics® v.5.6, has been used in this study. The gas exchange through a perforation was considered as a coupled transient mass and momentum transfer case. This model posited that the mass transport though the microperforation involves both convection and diffusion, and mass fraction of the different gases ω_i can be described using the Maxwell-Stefan equations:

$$\rho\frac{\partial\omega_i}{\partial t}+\nabla\left(-\rho\omega_i\sum_{j=1}^{n}D_{ij}\left(\nabla x_j+\left(x_j-\omega_j\right)\frac{\nabla p}{p}\right)\right)=-\rho u\nabla\omega_i \quad (1)$$

where t is the time, x_j is the mole fraction of species j, D_{ij} is the multicomponent Fick diffusivity matrix, p is the pressure, u is the velocity vector and ρ is the density, calculated from the ideal gas law. The binary gas diffusion coefficients for a gas pair ij, D_{ij}, are those recommended by Massman (1998):

$$D_{ij}=D_{ij}(T_o,p_o)\left(\frac{p_o}{p}\right)\left(\frac{T}{T_o}\right)^{1.81} \quad (2)$$

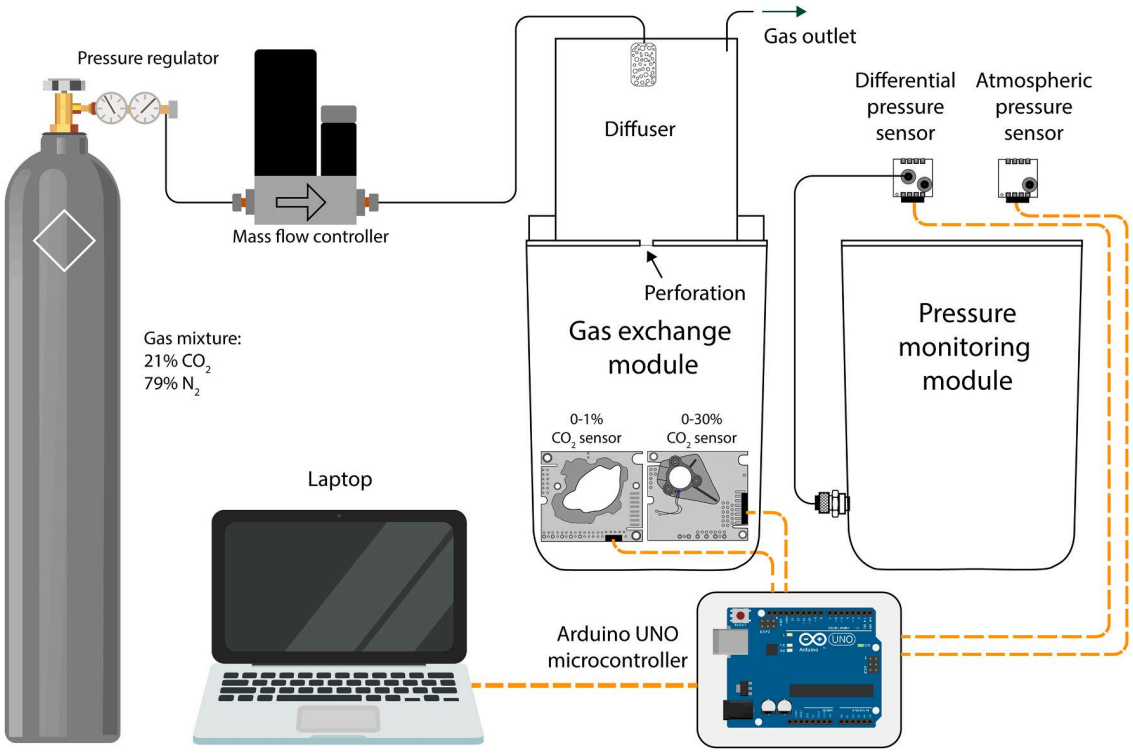

Fig. 1. Schematic diagram of the experimental set-up built to measure the CO_2 exchange through a microperforation and the changes in atmospheric pressure.

The transport momentum was described by Navier-Stokes equations for compressible Newtonian flow, considering constant temperature and force volume, dilatational viscosity and external forces equal to zero:

$$\rho\frac{\partial u}{\partial t}+\rho(u\nabla u)=-\nabla p+\nabla\left(\mu(\nabla u)-\frac{2}{3}\mu(\nabla u)I\right) \quad (3)$$

where I is the identity matrix and μ is the dynamic viscosity. These equations were solved together with the continuity equation that represents the conservation of mass:

$$\frac{\partial\rho}{\partial t}+\nabla(\rho u)=0 \quad (4)$$

The 3D physical system modeled recreates the exchange module of the experimental system (Fig. 2). Due to its rotational geometry, simulations were performed in a narrow section of one degree. Three domains were established: the chambers located above and below the perforation (Ω_1 and Ω_2, respectively), and the perforation path (Ω_3). The

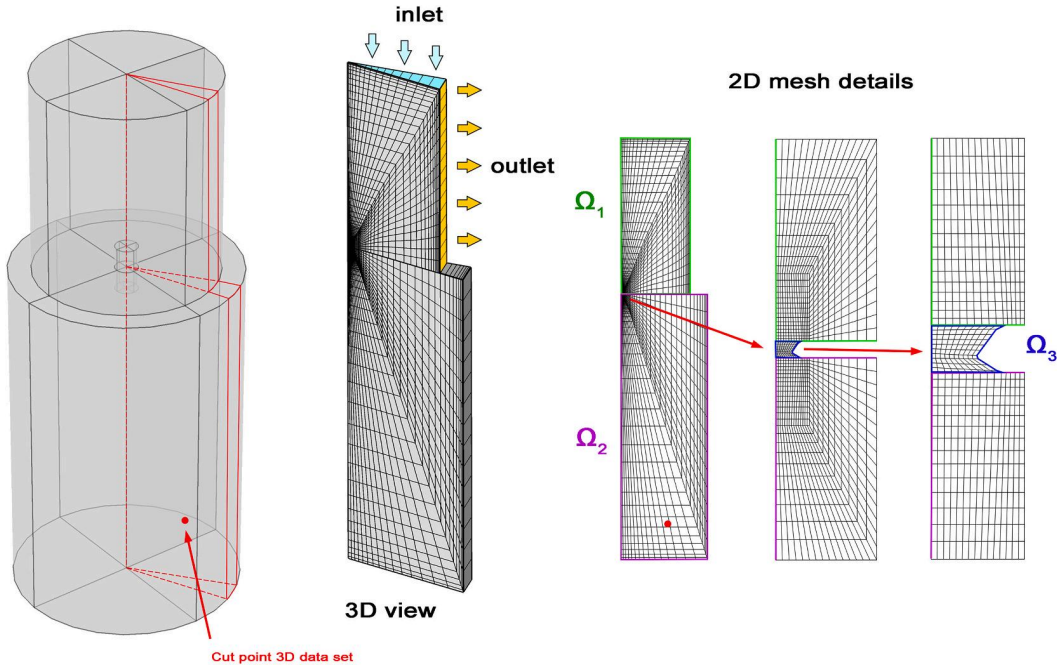

Fig. 2. Meshed computational domains.

initial pressure and the pressure in the surrounding environment varied depending on the simulated cases (section 2.3) and constitute a differential factor between this model and the one proposed by Gónzalez-Buesa and Salvador (2022) as it did not consider pressure changes. The following conditions are common to all cases: the initial temperature was 25 °C and constant over time; the initial gas composition in the upper chamber (Ω_1) was equal to that of the sweeping gas mixture (20.95 % CO_2-0.05 % O_2-0.79 % N_2) and in the lower chamber (Ω_2), it was considered similar to that of the air (0.05 % CO_2-20.95 % O_2-0,79 % N_2). Concerning the boundary conditions in the upper chamber (Ω_1), it was assumed that the gas mixture enters through the upper face and the gas exit through the lateral face (Fig. 2). Continuity between domains, symmetry on the internal faces, and impermeability in the remaining cases were considered. A mesh sensitivity analysis was conducted to find a suitable mesh size with the optimum computational efficiency for the optimization process. The mesh density was of 3850 elements and 3851 nodes. A finer mesh was created in the narrower region (Ω_3).

2.3. Cases addressed

The evolution of the gas composition on both sides of the perforation was simulated for the following situations involving a change in pressure: a) Fluctuations in atmospheric pressure. In these cases, the initial pressure in the whole system corresponded to the experimental data recorded at time zero by the atmospheric pressure sensor (Fig. 1). The boundary pressure of the upper chamber varies over time and corresponds to the values experimentally recorded by the sensors of the pressure monitoring module which were introduced into the model as inputs. b) Variation of atmospheric pressure with altitude. In these cases, the initial pressure in the system and the boundary pressure of the upper chamber correspond to the atmospheric pressure in places of different altitude, calculated with the barometric formula:

$$p[Pa] = p_o \cdot exp\left(-\frac{Mg}{RT}h\right) \quad (5)$$

where, p_o is the average sea level pressure (101,325 Pa), M is the molar mass of air (0.0289647 kg mol^{-1}), g is the gravitational acceleration (9.80665 m s^{-2}), R is the universal gas constant (8.314472 J $mol^{-1}{\cdot}K^{-1}$), T is the temperature at the standard sea-level conditions (288.15 K), and h is the altitude expressed in m. This pressure was considered to remain constant over time. c) Variation of barometric pressure during transport. The initial pressure in the system and the boundary pressure of the upper chamber was calculated from Eq. (5) according to the altitude of each point during the transport or obtained from direct pressure measurements. Three cases were considered: i) Road transport through a non-real route in which altitude changes were pre-established that could correspond to the ascent and descent of a mountain pass (considering a truck constant speed of 90 km h^{-1}, and 5% slope during 3 km). ii) Road transport through a real itinerary of a truck that followed the Ateca (Zaragoza)-Seville route in Spain. The pressure changes were determined in three different ways: by measuring and recording the pressure with a data logger (model EL-SIE-6+ EasyLog, Tonbridge, UK) located in the truck, from the altitude data recorded during the route by a GPS (Columbus P-10 P20, Columbus, Berlin, Germany) also located in the truck, and from the changes in altitude of the topography through which the road passes provided by Google Earth. iii) Air transport through a real itinerary of an aircraft that flew the Madrid-Rome route. The pressure changes were determined by measuring and recording the pressure with a data logger (model EL-SIE-6+ EasyLog, UK) located in the cabin.

3. Results

3.1. Fluctuations in atmospheric pressure

Fig. 3 shows the results obtained for a specific replica where the evolution of the atmospheric pressure recorded in the experimental system experienced strong pressure variations due to weather conditions (e.g., atmospheric pressure gain at 5 h, where rates over 0.4 Pa s^{-1} were reached). These pressure variations were incorporated into the model as a boundary condition. The evolution of the CO_2 concentration predicted by the model considering atmospheric pressure changes is shown as a solid line. The simulation data in the graph correspond to a point in the gas exchange chamber where the concentration is not affected by the proximity of the microperforation (0.1177 m). The experimentally measured CO_2 concentration follows a practically linear evolution deviating slightly from this behavior when the most abrupt changes in pressure occur. The model correctly predicted the experimental data with a Root Mean Squared Error, RMSE, of 0.01%. The resolution of the model considering constant atmospheric pressure predicts a CO_2 concentration below the experimental one with a RMSE of 0.11%. To illustrate how the gas exchange through the microperforation is affected by atmospheric pressure variations, Fig. 4 shows the CO_2 concentration and velocity profiles around the microperforation at two instants: points a and b, marked in Fig. 3. When the atmospheric pressure is stable (point a), the flow is predominantly diffusive. If there is an increase in pressure in the upper chamber (point b), the convective flow that is generated may reach velocities of up to 1 m s^{-1} to compensate for the difference in pressure on both sides of the microperforation. This macroscopic flow modifies the distribution of CO_2 around the perforation. Thus, at the top side of the microperforation, the CO_2 concentration lines are flatter and parallel to the film containing the microperforation, while at the bottom side of the microperforation the opposite occurs. These results are similar to those described by González-Buesa and Salvador (2022) where the convective flow was assumed to be generated by the metabolic activity of products with respiratory quotients less than 1. However, the magnitude of the convective flow was smaller than in the situation contemplated here, since the pressure changes did not exceed 0.07 Pa s^{-1}. Although quantitatively the differences between the two predictions, considering or not the pressure variations, are not very significant (Fig. 3), conceptually the results showed in Fig. 4 suggest that the effect of pressure should be explored for other cases where

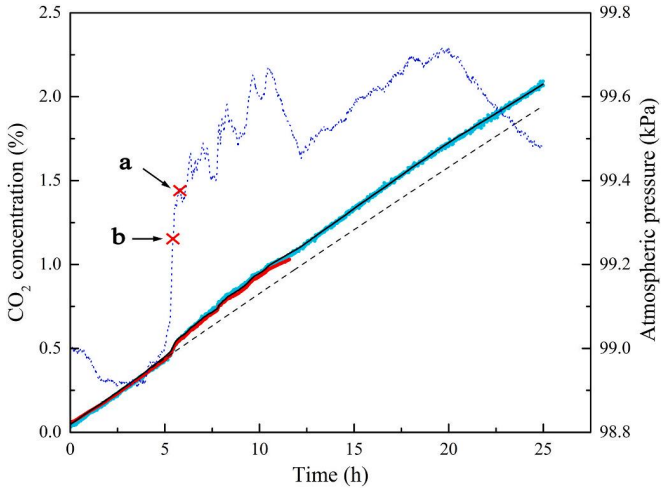

Fig. 3. Evolution of the CO_2 concentration in the lower chamber of the gas exchange module: experimental data (● for k30 sensor, ● for k33 sensor) and model prediction considering atmospheric pressure changes (——) and considering constant pressure (- - -). Barometric pressure data (.....).

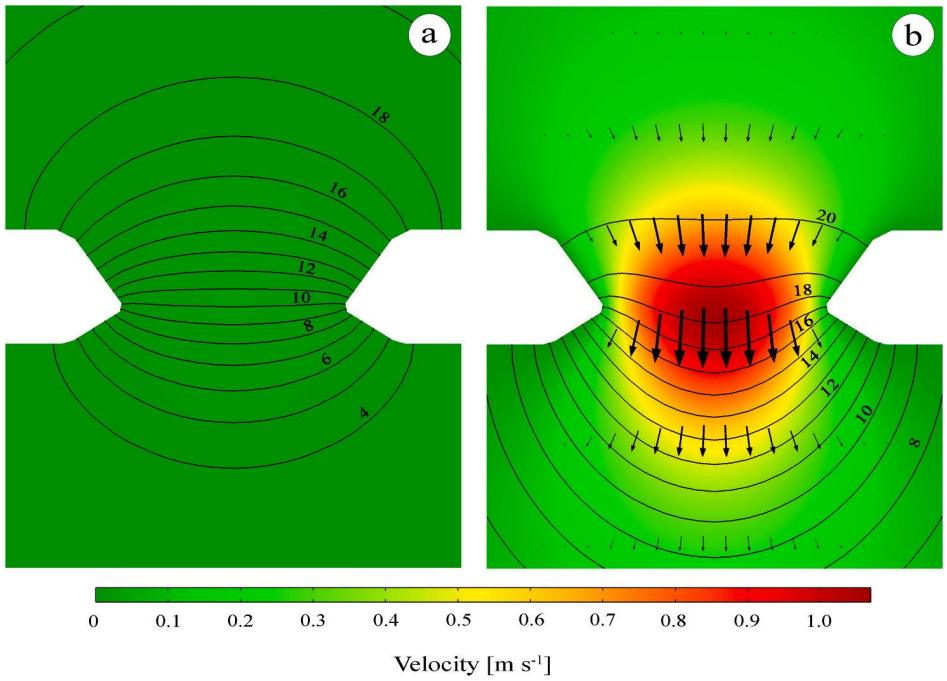

Fig. 4. Distribution of the CO_2 concentration (in lines) and velocity (in colours) around the microperforation at two different times corresponding to stable (a) and variable (b) atmospheric pressure.

fluctuations in atmospheric pressure are more pronounced, such as when the altitude changes.

3.2. Variation of atmospheric pressure with altitude

The gas exchange through microperforations has been simulated for locations at different altitudes. For this purpose, the initial pressure in the gas exchange module and the pressure outside of the upper chamber were considered to be that calculated using Eq. (5) for the altitudes of the following cities: Barcelona (12 m), Zaragoza (243 m), Madrid (667 m), Andorra la Vella (1,023 m), Quito (2,850 m), and Nagqu (4,491 m). In these cases, it has been considered that there are no atmospheric pressure changes due to weather conditions. Fig. 5 shows, at the different locations, the evolution of the CO_2 concentration in the lower chamber due to the gas exchange through the perforation. The CO_2 concentration increases exponentially towards the upper limit (20.95%), so that during the first 50 h the evolution of the CO_2 concentration could be considered approximately linear. After 300 h, the CO_2 concentration at sea level (14%) was almost one unit higher (14.9%) than that at an altitude of about 1,000 m, reaching values of 17.7% at one of the highest settlements in the world.

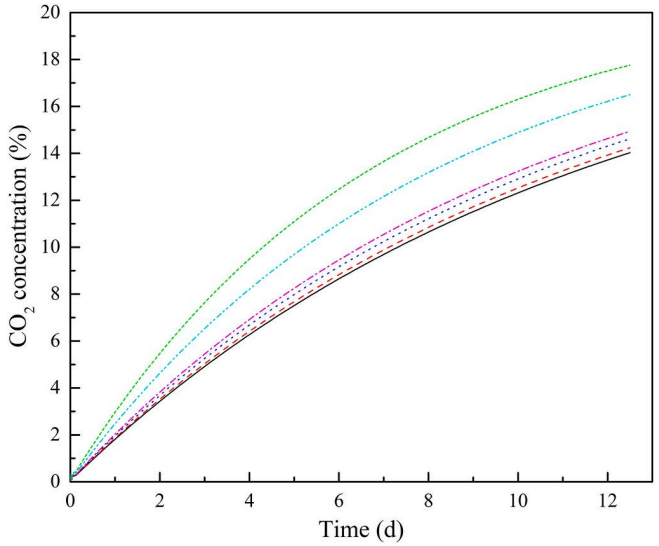

Fig. 5. Evolution of the CO_2 concentration predicted by the model for cities of different altitude: Barcelona (12 m altitude, ——), Zaragoza (243 m altitude, - - -), Madrid (667 m altitude, ...), Andorra (1023 m, -·- line), Quito (2850 m, -··-) and Nagqu (4491 m, ----).

3.3. Variation of atmospheric pressure during transport

Hypothetical transports were simulated between points located at the same altitude (250 m) following five different routes that would correspond to transports in which there is no change in altitude and in which mountain passes (altitude of 400 m) were ascended and descended (Fig. 6). For the different cases, the evolution of the pressure was included in the model as the boundary condition of the upper gas exchange chamber. The evolution that the model predicts of the CO_2 concentration in the lower gas exchange chamber is also shown in Fig. 6. As expected, the CO_2 concentration gradually increases approximately linearly during the route when there is no change in pressure (Route 1). In Routes 2 to 5, when the atmospheric pressure drops (ascent of the mountain pass), the CO_2 concentration in the measurement chamber barely changes. This is due to the convective flow that occurs in the opposite direction from the chamber with the lowest CO_2 concentration to the one with the highest concentration. This also causes a reduction in diffusive flow as the gradient decreases because the CO_2 concentration in the upper vicinity of the perforation becomes lower. When the pressure is considered constant (plateau), the gas exchange is only diffusive and the concentration of CO_2 increases gradually. When the pressure in the upper chamber increases (descent of the mountain pass), the convective flow of a gas rich in CO_2 tends to balance the pressure between both chambers, causing a sharp increase in the concentration of CO_2 in the lower chamber. Choosing one route or another can make a difference in the concentration of up to 2 units (in %) in the concentration of CO_2 during a transport of a few hours (3.37 h).

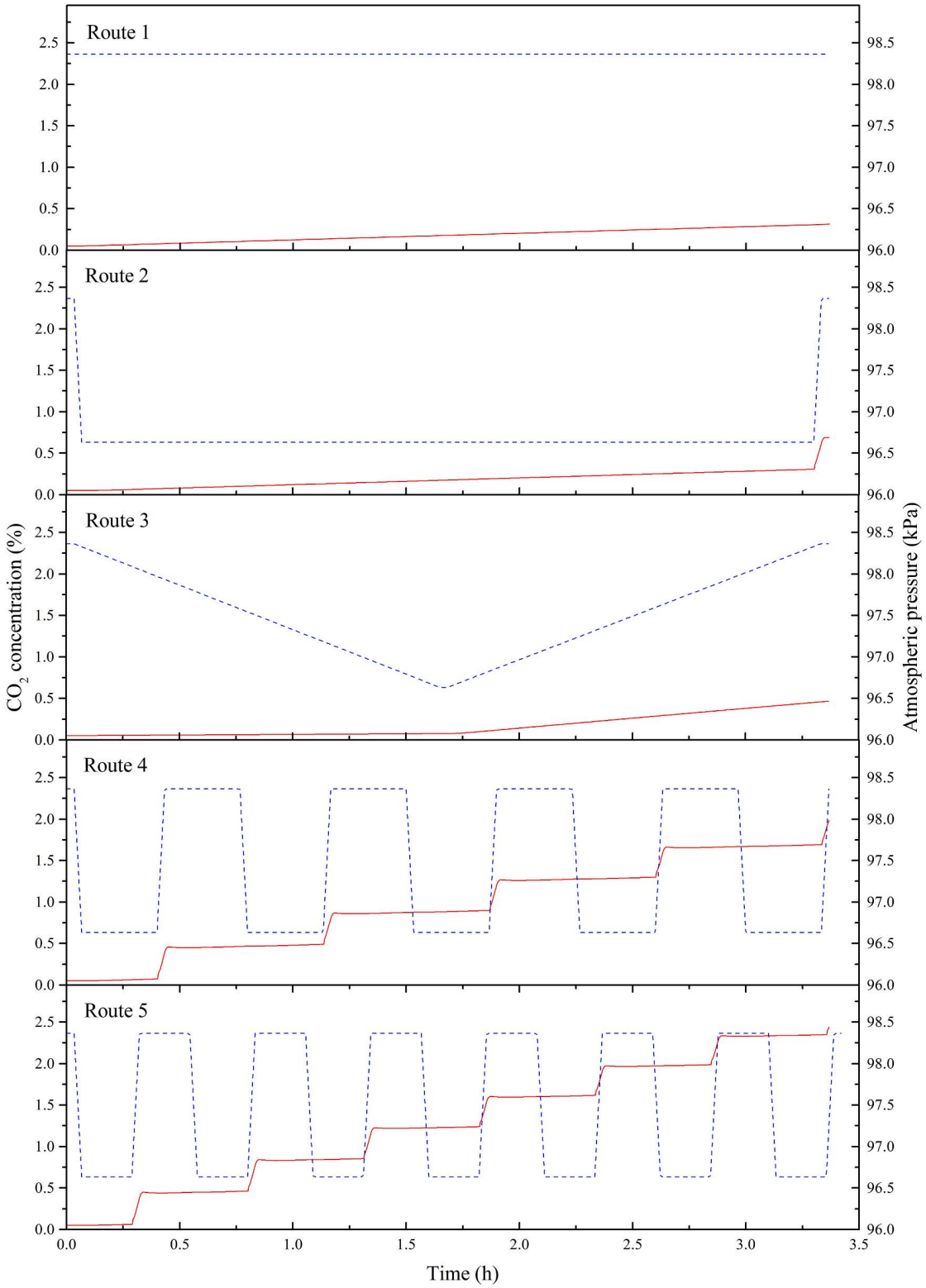

Fig. 6. Effect of the atmospheric pressure changes during different hypothetical transport routes on the evolution of the CO_2 concentration. Atmospheric pressure (- - -) and CO_2 concentration (——).

In order to advance in the study of the influence of transport by gas exchange through microperforations, a real case was analyzed which corresponded to road transport with a truck from Ateca (Zaragoza, Spain), which has an altitude of 603 m, to Seville (Spain), located almost at sea level (7 m). The route of 735 km had a duration of 10.27 h, taking into account the breaks that the truck driver must take in accordance with European Union rules for road transport workers. Fig. 7 shows the evolution of the atmospheric pressure during the route obtained in three different ways: directly from the pressure data recorded by a datalogger placed in the truck, from the altitude data provided by a GPS also placed

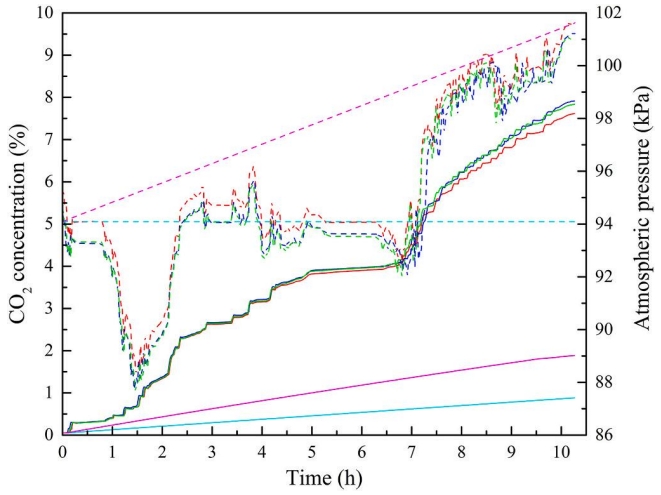

Fig. 7. Prediction of the evolution of CO_2 concentration during a real land route (Ateca-Sevilla in Spain) based on atmospheric pressure data acquired with a data logger (—), calculated from altitude data obtained with a GPS (—) and from altitude data provided by Google Earth (—). Results at constant pressure (—) and considering a linear variation of pressure (—) are also included. CO_2 concentration (solid lines) and atmospheric pressure data (dash lines).

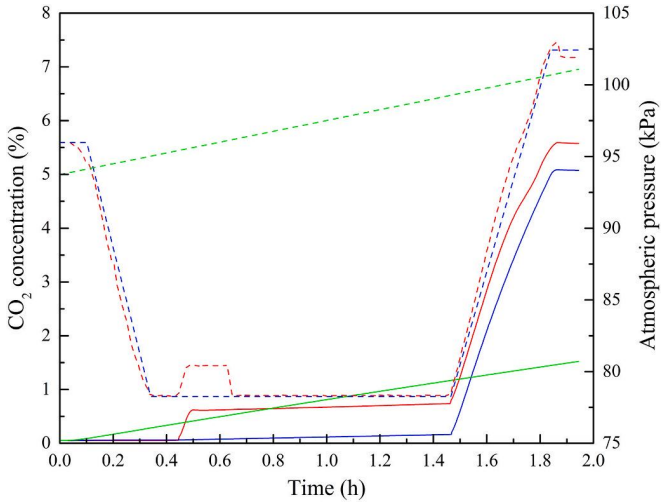

Fig. 8. Prediction of the evolution of the CO_2 concentration during an air transport (Madrid-Rome) based on real atmospheric pressure data acquired with a data logger (—), assuming that the pressure only changes during the ascent and descent of the aircraft (—), and considering a linear variation of the pressure (—). CO_2 concentration (solid lines) and atmospheric pressure data (dash lines).

in the truck, and from the altitude data of the topography through which the road passes. As can be seen, the pressure evolution is similar for the three cases, with logical differences arising from the fact that the data logger records pressure changes due to factors other than variations in altitude, such as those caused by weather conditions. In addition, the altitude of the road layout does not match exactly with the altitude of the land surface through which it runs. This is especially noticeable in tunnels and bridges. As in the previous cases, these pressure data were incorporated into the model as initial and boundary conditions, after which it was solved. The evolution of CO_2 in the lower chamber due to the diffusive and convective flow through the microperforation was very similar for the three cases. The concentration of CO_2 follows the behavior pattern described above for the hypothetical transport routes. When the pressure increases, there is an increase in the concentration of CO_2; when the pressure decreases, the concentration hardly changes; and when the pressure is constant, the concentration of CO_2 increases smoothly by diffusive flow. Fig. 7 also shows the evolution of the CO_2 concentration if the constant atmospheric pressure is considered throughout the route (94,092 Pa), and therefore the gas exchange through the perforation is only due to diffusion. The concentration of CO_2 at the end of the transport is very different when the effect of pressure is neglected (0.88%) and when the pressure-driven flow is taken into account (7.62, 7.91 and 7.83% depending on the system used to quantify the pressure changes). If the atmospheric pressure is considered to change linearly between the pressure of Ateca (94,002 Pa) and that of Seville (101,624 Pa), the CO_2 concentration differs greatly from that obtained considering all the altitude fluctuations, reaching a CO_2 concentration of only 1.89% at the end of the route.

Finally, since some fruits and vegetables may be transported by air and are therefore subjected to the pressure changes involved in an aircraft route, it was considered interesting to analyze the repercussion that pressure changes during a flight would have on the gas exchange through microperforations. For this purpose, a flight from Madrid to Rome was simulated. This simulation has been performed in three ways: i) from real pressure data recorded with a pressure data logger placed in the aircraft cabin, ii) from pressure data considering a constant climb rate of the aircraft of 2 m s^{-1} and a descent rate of 1.7 m s^{-1}, maintaining an altitude of around 2,180 m during the flight, and iii) assuming that the pressure varies linearly during the duration of the flight between the pressure of Madrid and Rome calculated by Eq. (5). Following the same methodology described above, the pressure data was incorporated into the mathematical model and the evolution of the CO_2 concentration in the lower chamber of the gas exchange module was simulated. The results obtained are shown in Fig. 8 together with the evolution of the pressure for the three cases. The concentration of CO_2 follows the same pattern when changing the pressure as that previously described for road transport. The actual pressure data record showed an unexpected increase in cabin pressure of 2,082 Pa, which occurred between 1,600 and 2,500 s once the pressure had stabilized. Subsequently, the pressure stabilized again at around 78,255 Pa. This change in pressure resulted in a sudden increase in the concentration of CO_2 from 0.05 to 0.63%. This pressure variation does not occur in the simulation carried out with the fictitious pressure data in which the pressure between the ascent and descent of the aircraft was assumed to be constant, and marks the differences between these two cases. Therefore, at the end of the flight, the CO_2 concentration was 5.58% for the simulated case with real pressure data, and 5.08% for the simplified case ii). On the other hand, it is worth noting that the concentration of CO_2 at the end of the simulation was only 1.52% for case iii) in which a linear evolution was assumed between the atmospheric pressure of the cities of origin and destination. This confirms the results obtained in the Ateca-Seville truck transport suggesting that all pressure fluctuations must be taken into account, not only the initial and final conditions.

4. Discussion

These results indicate that the contribution of pressure-driven flow to the total gas exchange through microperforations can be important in a microperforated package. The elevation of the package location or the fluctuations in barometric pressure during the transport of these products due to changes in altitude are factors that significantly affect the convective flow. In a real transport of respiring products in MAP with microperforated films, the differences between considering the pressure variable or constant would not be so pronounced as in the cases discussed above. There are two main causes that would reduce the differences. First, the optimal atmosphere for the preservation of many fruits and vegetables results in lower concentration gradients through the microperforation than those simulated here (Kader et al., 1989). Secondly, it is possible that there would be more than one microperforation and then the pressure-driven flow would be distributed among the

microperforations. This could justify the assumption of some authors of only considering diffusive flow when the number of microperforations is high (Xanthopoulos et al., 2012). Another factor that can influence the effect of the convective flow on the gas composition inside the package is the size of the perforation. That is why the convective flow is neglected for perforations larger than 300 μm (Giannoulis et al., 2017; Lange et al., 2000). Sometimes the convective flow is neglected even for small leaks and is compensated with a correction term to take into account the fact that the air around the perforation may not be in equilibrium with the surrounding bulk air (Chung et al., 2003; Ghosh and Anantheswaran, 2001; Mistriotis et al., 2016).

However, there are other phenomena that can take place during the actual transport of respiring products in MAP that can contribute to pressure drops or rise inside the package, increasing the convective flow through the microperforations and, consequently, the differences between considering constant or variable pressure. An example is the respiratory activity of products with a respiratory quotient different than 1 (González-Buesa and Salvador, 2022). Some authors have analyzed and modeled other factors that generate pressure drops such as the condensation of moisture, the absorption of CO_2 and other species by the water condensed or by the water contained in the product, the use of moisture absorbers or gas scavengers (Jalali et al., 2019; Lee, 2016). However, they have not related these factors to a change in the flow through the microperforations, since for this it is necessary to contemplate the spatial dependence of the gas concentrations in the headspace.

5. Conclusions

The 3D coupled mass and momentum transfer computational model, based on Maxwell-Stefan and Navier-Stokes equations, has adequately predicted the gas exchange through microperforations, considering changes in atmospheric pressure, and the spatial-time and pressure dependence of the gas composition, even when the atmospheric pressure changes are high (around 0.4 Pa s^{-1}). Therefore, the model has been considered valid for simulating how other pressure changes affect the gas exchange through microperforations, such as those caused by changes in altitude during road or air transport. Since pressure changes during road transport in medium mountain routes or air transport are higher than weather related pressure changes, the results reported here should be treated with caution. However, the simulations of different locations and of different real and fictitious transport routes, both on land and in the air, have made it possible to establish the response pattern of gaseous exchange to changes in altitude and to quantify its effect. From these simulations, it can be concluded that pressure changes outside a microperforated package containing respiring products have a significant effect. Mathematical models that intend accurately and rigorously to predict the evolution of the gas composition inside a microperforated package must consider, in addition to the diffusive flow, the convective flow given that several factors can generate pressure changes inside and outside the package.

In future works, these conclusions will be experimentally corroborated for the reasons explained. However, in this work we wanted to isolate the effect of pressure changes outside the container on gas exchange through microperforations, which would have been impossible to achieve experimentally in a real package containing products. The respiratory activity of the products, normally with rates of O_2 consumption above those of CO_2 production, and the different permeation rates of O_2 and CO_2 through the package, among other causes, would generate a pressure drop inside the package. Therefore, the convective flow would balance the pressure without it being possible to differentiate the contribution of the pressure changes inside the package from those outside.

CRediT authorship contribution statement

Sara Vega-Diez: Writing – review & editing, Visualization, Software, Investigation, Formal analysis. **María Luisa Salvador:** Writing – review & editing, Writing – original draft, Visualization, Supervision, Methodology, Conceptualization. **Jaime González-Buesa:** Writing – review & editing, Supervision, Resources, Methodology, Investigation, Funding acquisition, Conceptualization.

Declaration of competing interest

The authors declare that they have no known competing financial interests or personal relationships that could have appeared to influence the work reported in this paper.

Data availability

Data will be made available on request.

Acknowledgements

This work was supported by the Ministerio de Ciencia e Innovación of Spain (projects PID 2022-142850OR-I00 and PID 2019–108080RR-100, and pre-doctoral grant PRE 2022-000492 to Sara Vega-Diez) and the Instituto Nacional de Investigación y Tecnología Agraria y Alimentaria of Spain (INIA-DOC fellowship to J. González-Buesa). We would like to thank Frutas Hermanos Aguilar S.L. (Ateca, Spain), Transportes Cruz Lozano (Ateca, Spain), Dr. Sergio Sánchez, and David Vega for their help during the data acquisition in the road and air transport routes.

References

Belay, Z.A., Caleb, O.J., Opara, U.L., 2016. Modelling approaches for designing and evaluating the performance of modified atmosphere packaging (MAP) systems for fresh produce: a review. Food Packag. Shelf Life 10, 1–15. https://doi.org/10.1016/j.fpsl.2016.08.001.

Castellanos, D.A., Cerisuelo, J.P., Hernandez-Muñoz, P., Herrera, A.O., Gavara, R., 2016. Modelling the evolution of O_2 and CO_2 concentrations in MAP of a fresh product: application to tomato. J. Food Eng. 168, 84–95. https://doi.org/10.1016/j.jfoodeng.2015.07.019.

Chung, D., Papadakis, S.E., Yam, K.L., 2003. Simple models for evaluating effects of small leaks on the gas barrier properties of food packages. Packag. Technol. Sci. 16, 77–86. https://doi.org/10.1002/pts.616.

Del-Valle, V., Almenar, E., Lagarón, J.M., Catalá, R., Gavara, R., 2003. Modelling permeation through porous polymeric films for modified atmosphere packaging. Food Addit. Contam. 20, 170–179. https://doi.org/10.1080/0265203021000042869.

Fishman, S., Rodov, V., Ben-Yenoshua, S., 1996. Mathematical model for perforation effect on oxygen and water vapor dynamics in modified-atmosphere packages. J. Food Sci. 61, 956–961. https://doi.org/10.1111/j.1365-2621.1996.tb10910.x.

Ghosh, V., Anantheswaran, R.C., 2001. Oxygen transmission rate through microperforated films: measurement and model comparison. J. Food Process. Eng. 24, 113–133. https://doi.org/10.1111/j.1745-4530.2001.tb00535.x.

Giannoulis, A., Mistriotis, A., Briassoulis, D., 2017. 3D numerical simulations as optimization tool for the design of novel EMAP systems. Comput. Electron. Agric. 143, 119–129. https://doi.org/10.1016/j.compag.2017.10.004.

González, J., Ferrer, A., Oria, R., Salvador, M.L., 2008. Determination of O_2 and CO_2 transmission rates through microperforated films for modified atmosphere packaging of fresh fruits and vegetables. J. Food Eng. 86, 194–201. https://doi.org/10.1016/j.jfoodeng.2007.09.023.

González-Buesa, J., Ferrer-Mairal, A., Oria, R., Salvador, M.L., 2009. A mathematical model for packaging with microperforated films of fresh-cut fruits and vegetables. J. Food Eng. 95, 158–165. https://doi.org/10.1016/j.jfoodeng.2009.04.025.

González-Buesa, J., Salvador, M.L., 2022. A multiphysics approach for modeling gas exchange in microperforated films for modified atmosphere packaging of respiring products. Food Packag. Shelf Life 31, 100797. https://doi.org/10.1016/j.fpsl.2021.100797.

Jalali, A., Rux, G., Linke, M., Geyer, M., Pant, A., Saengerlaub, S., Mahajan, P., 2019. Application of humidity absorbing trays to fresh produce packaging: mathematical modeling and experimental validation. J. Food Eng. 244, 115–125. https://doi.org/10.1016/j.jfoodeng.2018.09.006.

Kader, A.A., Zagory, D., Kerbel, E.L., Wang, C.Y., 1989. Modified atmosphere packaging of fruits and vegetables. Crit. Rev. Food Sci. Nutr. 28, 1–30. https://doi.org/10.1080/10408398909527490.

Lange, J., Büsing, B., Hertlein, J., Hediger, S., 2000. Water vapour transport through large defects in flexible packaging: modeling, gravimetric measurement and magnetic resonance imaging. Packag. Technol. Sci. 13, 139–147. https://doi.org/10.1002/1099-1522(200007)13:4<139::AID-PTS507>3.0.CO;2-E.

Larsen, H., Liland, K.H., 2013. Determination of O_2 and CO_2 transmission rate of whole packages and single perforations in micro-perforated packages for fruit and vegetables. J. Food Eng. 119, 271–276. https://doi.org/10.1016/j.jfoodeng.2013.05.035.

Lee, D.S., 2016. Carbon dioxide absorbers for food packaging applications. Trends Food Sci. Technol. 57, 146–155. https://doi.org/10.1016/j.tifs.2016.09.014.

Lee, D.S., Renault, P., 1998. Using pinholes as tools to attain optimum modified atmospheres in packages of fresh produce. Packag. Technol. Sci. 11, 119–130. https://doi.org/10.1002/(SICI)1099-1522(199805/06)11:3<119::AID-PTS421>3.0.CO;2-N.

Massman, W.J., 1998. A review of the molecular diffusivities of H_2O, CO_2, CH_4, CO, O_3, SO_2, NH_3, N_2O, NO, and NO_2 in air, O_2 and N_2 near STP. Atmos. Environ. 32, 1111–1127. https://doi.org/10.1016/S1352-2310(97)00391-9.

Mistriotis, A., Briassoulis, D., Giannoulis, A., D'Aquino, S., 2016. Design of biodegradable bio-based equilibrium modified atmosphere packaging (EMAP) for fresh fruits and vegetables by using micro-perforated poly-lactic acid (PLA) films. Postharvest Biol. Technol. 111, 380–389. https://doi.org/10.1016/j.postharvbio.2015.09.022.

Pandey, S.K., Goswami, T.K., 2012. Modelling perforated mediated modified atmospheric packaging of capsicum. Int. J. Food Sci. Technol. 47, 556–563. https://doi.org/10.1111/j.1365-2621.2011.02877.x.

Paul, D.R., Clarke, R., 2002. Modeling of modified atmosphere packaging based on designs with a membrane and perforations. J. Membr. Sci. 208, 269–283. https://doi.org/10.1016/S0376-7388(02)00303-4.

Ramos, A.V., Sousa-Gallagher, M.J., Oliveira, J.C., 2019. Effect of hydrodynamic conditions and geometric aspects on the permeance of perforated packaging films. Food Bioprocess Technol. 12, 1527–1536. https://doi.org/10.1007/s11947-019-02309-8.

Ratti, C., Rabie, H.R., Raghavan, G.S.V., 1998. Modelling modified atmosphere storage of fresh cauliflower using diffusion channels. J. Agric. Eng. Res. 69, 343–350. https://doi.org/10.1006/jaer.1997.0254.

Renault, P., Houal, L., Jacquemin, G., Chambroy, Y., 1994. Gas exchange in modified atmosphere packaging. 2: experimental results with strawberries. Int. J. Food Sci. Technol. 29, 379–394. https://doi.org/10.1111/j.1365-2621.1994.tb02080.x.

Rennie, T.J., Tavoularis, S., 2009a. Perforation-mediated modified atmosphere packaging. Part I. Development of a mathematical model. Postharvest Biol. Technol. 51, 1–9. https://doi.org/10.1016/j.postharvbio.2008.06.007.

Rennie, T.J., Tavoularis, S., 2009b. Perforation-mediated modified atmosphere packaging. Part II. Implementation and numerical solution of a mathematical model. Postharvest Biol. Technol. 51, 10–20. https://doi.org/10.1016/j.postharvbio.2008.06.012.

Singh, R.K., Singh, N., 2005. Quality of packaged foods. In: Han, J.H. (Ed.), Innovations in Food Packaging. Academic Press, London, pp. 24–44. https://doi.org/10.1016/B978-0-12-311632-1.X5031-1.

Sonawane, A.D., Pathak, N., Weltzien, C., Mahajan, P., 2022. Ethylene permeance through perforated packaging film: modelling and effect of air velocity, temperature, film thickness and perforation diameter. Food Packag. Shelf Life 34, 100961. https://doi.org/10.1016/j.fpsl.2022.100961.

Sousa-Gallagher, M.J., Mahajan, P.V., 2013. Integrative mathematical modelling for MAP design of fresh-produce: theoretical analysis and experimental validation. Food Control 29, 444–450. https://doi.org/10.1016/j.foodcont.2012.05.072.

Winotapun, C., Issaraseree, Y., Sirirutbunkajal, P., Leelaphiwat, P., 2023. CO_2 laser perforated biodegradable films for modified atmosphere packaging of baby corn. J. Food Eng. 341, 111356 https://doi.org/10.1016/j.jfoodeng.2022.111356.

Xanthopoulos, G., Koronaki, E.D., Boudouvis, A.G., 2012. Mass transport analysis in perforation-mediated modified atmosphere packaging of strawberries. J. Food Eng. 111, 326–335. https://doi.org/10.1016/j.jfoodeng.2012.02.016.